Available online at www.sciencedirect.com
SCIENCE DIRECT®
International Journal of Thermal Sciences 42 (2003) 153–168
International Journal of Thermal Sciences
www.elsevier.com/locate/ijts

Numerical investigation of alternative process conditions for influencing the thermal history of spray deposited billets

Olaf Meyer, Udo Fritsching *, Klaus Bauckhage

University Bremen, SFB 372 "Spray Forming", Badgasteiner Str. 3, 28359 Bremen, Germany

Received 20 September 2001; accepted 12 March 2002

Abstract

In spray forming, during the spray deposition process and the subsequent cooling period a time dependent temperature field develops within the product and the solidification of the remaining liquid fraction takes place. In this paper, the time dependent thermal conditions and solidification behaviour in spray formed billets are investigated. A transient numerical simulation is carried out and compared with experimental results. A description of the relevant model and the developed program will be given and an investigation of the influence of different process parameters on the time dependent temperature field and the solidification history within billets are shown. The numerical model is based on a single-phase formulation of the energy equation. A non-orthogonal coordinate system is used for grid generation within the time dependent growing shape of the billet. Temperature measurements are carried out within the substrate and also in the lower part of the billet in the spray forming process. The material discussed throughout this contribution is CuSn6 (2.1020).

Résumé

Lors de la mise en oeuvre de la technologie de « spray forming », pendant la phase de dépôt et la période de refroidissement, le champ de température au sein du produit évolue au cours du temps et la partie de matériau restant sous forme liquide se solidifie. Cette publication analyse l'évolution des conditions thermiques au cours du temps ainsi que le processus de solidification lors de la formation de barres métalliques par la technologie de spray forming. Une simulation numérique de la phase de transition est réalisée et comparée avec les résultats expérimentaux. Le modèle utilisé et le programme développé sont décrits, et une étude des de l'influence des paramètres principaux sur le temps caractéristique de l'évolution du champ de température et le processus de solidification au sein des barres est faite. Le modèle numérique est basé sur une formulation uniphasique de l'équation de conservation de l'énergie. Le maillage de la forme de la pièce—forme qui se modifie au cours du processus—est réalisé à l'aide d'un système de coordonnées non-orthogonales afin de faciliter les comparaisons. Des mesures de température sont effectuées à l'intérieur du substrat ainsi que dans la partie inférieure de la barre métallique. Le métal considéré dans l'ensemble de l'article est l'alliage CuSn6 (2.1020).

Keywords: Spray forming; Solidification; Billet; Numerical simulation; Temperature measurement; CuSn6

Mots-clés : Spray forming ; Solidifie ; Barres ; Simulation numérique ; Mesures de température ; CuSn6

1. Introduction

The spray forming process enables near-net-shape production of homogeneous deposits and products. One of the most common and commercially successful spray formed geometries is the cylindrical billet, which may be spray formed up to 2 m in height and 0.5 m in diameter. Examples for commercial production from spray formed billet-shaped products include the production of AlSi cylinder liners for automotive industry [1], the spray forming of billets of copper based alloys [2] and tool steels [3].

During deposition and cooling of the sprayed geometry, a time dependent temperature field develops within the billet. At the same time, the solidification of the remaining liquid fraction within this deposit takes place. The time dependent temperature field and solidification history within a spray-deposited billet and within the spray essentially influence

* Corresponding author.
E-mail addresses: om@iwt.uni-bremen.de (O. Meyer), ufri@iwt.uni-bremen.de (U. Fritsching).

1290-0729/02/$ – see front matter
PII: S1290-0729(02)00015-7

Nomenclature

c	specific heat	$J \cdot kg^{-1} \cdot K^{-1}$
f	volumetric phase fraction	
H	volumetric enthalpy	$J \cdot m^{-3}$
k	heat transition coefficient	$W \cdot m^{-2} \cdot K^{-1}$
L	latent heat of solidification	$kJ \cdot kg^{-1}$
$\dot{q}_\alpha$	heat flux due to convection	$W \cdot m^{-2}$
$\dot{q}_\varepsilon$	heat flux due to radiation	$W \cdot m^{-2}$
$\dot{q}_k$	heat flux over the deposit/billet contact zone	$W \cdot m^{-2}$
T	temperature	K
T_{ref}	reference temperature	K
t	time	s

Greek symbols

α	heat transfer coefficient	$W \cdot m^{-2} \cdot K^{-1}$
$\alpha 1$	heat transfer coefficient during spray time	$W \cdot m^{-2} \cdot K^{-1}$
$\alpha 2$	heat transfer coefficient during cooling time	$W \cdot m^{-2} \cdot K^{-1}$
ε	emissivity	
Φ	Kirchhoff transformed temperature	$W \cdot m^{-1}$
λ	thermal conductivity	$W \cdot m^{-1} \cdot K^{-1}$
ρ	density	$kg \cdot m^{-3}$
σ	Stefan–Boltzmann constant	$W \cdot m^{-2} \cdot K^4$

Subscripts

b	billet
ch	chamber wall
l	liquid phase
s	solid phase
sub	substrate
u	ambient air
w	billet surface

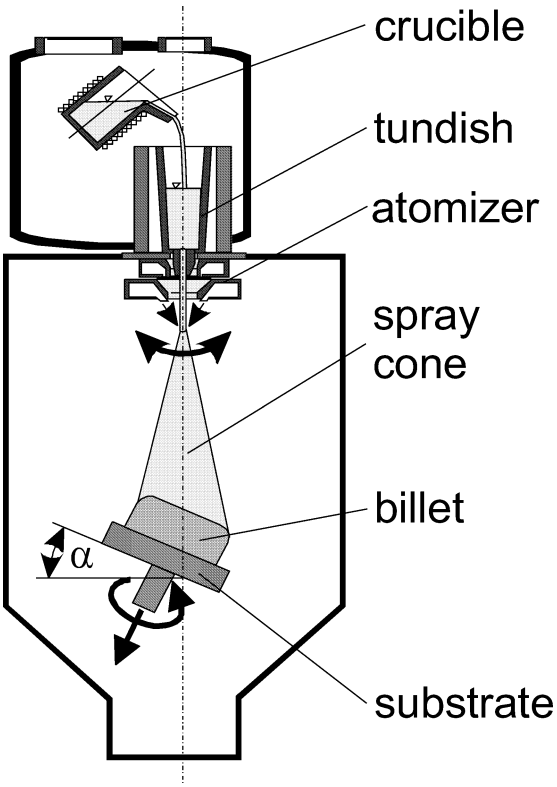

Fig. 1. Schematic diagram of the spray forming process configuration.

the material properties and the microstructure of the final product [4–6].

The thermal history of a spray formed billet depends on a great number of material and process parameters. In Fig. 1 a schematic diagram of the spray forming process configuration used in Bremen is shown. After melting in a crucible under inert gas atmosphere (argon or nitrogen), the overheated melt flows through the tundish and builds a free falling liquid jet. A system of gas nozzles (free-fall atomizer) located below the tundish focuses jets onto this melt stream. In the atomization zone, the metal jet is disintegrated into a spray of different sized droplets. The gas flow accelerates the droplets towards the substrate. In the spray, an intense transfer of heat and momentum takes place between droplets and gas. The droplets are partially solidified when they are collected on a substrate and build the deposit. For the production of a billet, a rotating disc is used as substrate.

Some important parameters of the spray forming process are the melt superheat in the crucible, the material properties of the alloy, and the gas and metal flow rates. By varying the atomization conditions, the local particle size distribution, the mass flux, and the relative velocity between the gas and the particles can be influenced. In this way the temperature of the particles and the liquid fraction within the spray cone are controlled [7–10].

The atomization process (for a fixed nozzle geometry) is influenced mainly by the gas to metal mass flow ratio (GMR). The thermal state of the metal mass (in terms of temperature and solidification state) impacting on the billet surface and the local mass distribution in the spray are additionally affected by the spraying distance and the scanning motion of the spray. The resulting geometry of the billet is determined by the mass flux distribution in the spray, the local particle sticking efficiency [11], the scanning motion of the spray, and the substrate motion.

In this paper, the time dependent thermal conditions in a billet during the spray period and the subsequent cooling period in the spray forming process are investigated. Therefore, transient numerical simulations of the thermal conditions are conducted. The aim is to investigate the qualitative influence of different process parameters on the temperature history of spray formed billets. Results of

computations are compared with temperature measurements performed in-situ during the spray forming process. The material used and discussed throughout this contribution is the copper alloy $CuSn_6$.

The most important parameters for an energy balance of a growing billet in spray forming are:

- the geometry of the billet,
- the spray enthalpy and mass flux distribution in the spray impacting onto the surface of the growing billet,
- the heat flux from the surface of the billet to the substrate and to the surrounding gas environment, and
- the material properties of the alloy.

Investigating how different parameters influence the temperature history and thermal distribution is an important input for the determination of how the resulting material properties can be controlled by varying the process boundary conditions.

Reliable temperature information for process control and optimization within the entire billet during the deposition and the cooling process are not easy to obtain. Only the temperatures within different sections of the deposit may be collected by common measurement methods. Some previous experimental investigations using pyrometer measurements and thermocouples have been performed. For example, temperature measurements on the billets surface have been done using a pyrometer [11,12], and plunging of thermocouples into the sprayforms was performed in [12]. Furthermore, temperature measurements can be acquired within the substrate and the lower part of the deposit by thermocouples [5,7,13]. Yet, a large number of experiments are necessary to derive the influence of the most important parameters in the spray forming process. Thus, numerical simulation of the thermal history within billets is a viable alternative to investigate of the dependence of process parameters on the resulting temperature history. By numerical modeling and simulation, it is possible to investigate the thermal conditions (temperature, liquid fraction) within the entire billet during the spray forming process. Measurement results can then be used to verify the models. The final aim of the simulation is to obtain quantitative predictions of the thermal history within the billet depending on different process parameters. Such a prediction may help to realize a control algorithm of the spray forming process. Some research has been published on thermal simulations of spray formed deposits [13–19]. The authors used different simplifying model assumptions and solution methods. Some of these simulations are used as a starting point for further studies, e.g. modelling the thermal residual stresses in the deposit [18, 19]. In some publications, the geometry of the growing billet is simplified for the simulation of the thermal conditions [15,16], some differing geometries (strips, gaussian deposit) are considered [13,17,19], or only the cooling behaviour of the deposit after the spraying period is considered in the simulation [19]. With the method introduced in this paper, a high flexibility with respect to the real geometry of the billet is reached. Also, in previous literature there are differences in the consideration of the impacting mass flux. It can be distinguished between single droplets impacting on the surface [13], the continuous growth of the deposit surface [14], and gradually added layers [15,17,18]. The last mentioned method is also used in this work. Thereby, a thermal model is derived which is fitted to the process boundary conditions within billet production.

2. Model formulation

2.1. Modeling of transient heat conduction with phase change

The numerical model derived here takes into account the time dependent geometry of the growing billet during the spray forming process. For the computation of the thermal history, the problem of transient heat conduction with phase change in the domain of a spray deposited billet of realistic geometry is solved. The developed program is based on a single-phase formulation of the energy equation and model of the solidification process with an appropriate source term [20,21]. It is assumed that the spray which builds the billet consists of a mixture of solid, semi-solid and liquid droplets and particles. The impacting semi-solid particles build a mixed layer on top of the billet—the so-called "mushy zone". In this layer, further solidification of the liquid metal takes place. Neglecting convection effects, the energy equation may be written as:

$$\frac{\partial}{\partial t}(H) = \nabla(\lambda \nabla T) \tag{1}$$

in which H is the total enthalpy of the liquid and the solid part of the alloy, T is the temperature, and λ the thermal conductivity of the mixture. The total enthalpy of the mixture can be formulated as [21,22]

$$H = f_s H_s + f_l H_l \tag{2}$$

with

$$H_s = \int_{T_{\text{ref}}}^{T} \rho_s c_s \, \mathrm{d}T \tag{3}$$

and

$$H_l = \int_{T_{\text{ref}}}^{T} \rho_l c_l \, \mathrm{d}T + \rho_l L \tag{4}$$

where f is the volumetric phase fraction, ρ is the density, c is the specific heat, L is the latent heat of solidification, and T_{ref} is a reference temperature. The subscript 's' refers to the solid phase, and similarly 'l' to the liquid phase. In this formulation of the enthalpy, a different composition of the two phases is taken into consideration. An assumption of

the model is that the densities of both phases are equal and independent of temperature. Hence from Eqs. (2)–(4) and noting that

$$f_l + f_s = 1 \tag{5}$$

the enthalpy of the mixture may be expressed as

$$H = \rho(1 - f_l)\int_{T_{\text{ref}}}^{T} c_s \,\mathrm{d}T + \rho f_l \int_{T_{\text{ref}}}^{T} c_l \,\mathrm{d}T + \rho f_l L \tag{6}$$

According to Eq. (6), the enthalpy of the mixture is only a function of temperature and liquid fraction. This leads to the following derivative:

$$\frac{\partial H(f_l, T)}{\partial t} = \frac{\partial H}{\partial T}\frac{\partial T}{\partial t} + \frac{\partial H}{\partial f_l}\frac{\partial f_l}{\partial t} \tag{7}$$

Substituting Eqs. (6) and (7) into Eq. (1), and assuming a reference temperature of $T_{\text{ref}} = 0$, the governing equation may be expressed as

$$\rho\big\{(1 - f_l)c_s + f_l c_l\big\}\frac{\partial T}{\partial t} = \nabla(\lambda \nabla T) + S \tag{8}$$

where the source term S is defined as

$$S = -\rho\left\{\int_{T_{\text{ref}}}^{T} (c_l - c_s)\,\mathrm{d}T + L\right\}\frac{\partial f_l}{\partial t} \tag{9}$$

This form of the conservation equation is used for the numerical solution of the problem. The heat conduction term in Eq. (8) is non-linear, when the thermal conductivity is a function of temperature. To linearize this term, a Kirchhoff transformation of the temperature [20,23]

$$\Phi = \int_{T_{\text{ref}}}^{T} \lambda\{T\}\,\mathrm{d}T \tag{10}$$

is used. For further simplification of the problem, the temperature field within the ingot is assumed to be axisymmetric. Because of this assumption and the Kirchhoff transformation (10), the governing equation (8) can be written as

$$\frac{\rho[(1 - f_l)c_s + f_l c_l]}{\lambda\{T\}}\frac{\partial \Phi}{\partial t} = \left(\frac{\partial^2 \Phi}{\partial x^2} + \frac{\partial^2 \Phi}{\partial r^2} + \frac{1}{r}\frac{\partial \Phi}{\partial r}\right) - \rho\left\{\int_{T_{\text{ref}}}^{T} (c_l - c_s)\,\mathrm{d}T + L\right\}\frac{\partial f_l}{\partial t} \tag{11}$$

where z and r are cylindrical coordinates. Additionally, the specific heat is assumed to be independent of phase ($c_l\{T\} = c_s\{T\}$). The partial differential equation (11) needs to be solved with appropriate boundary and initial conditions.

At the beginning of a spray forming experiment for billet production, the melt is impacting on a rotating substrate. Heat transfer takes place between the substrate and the billet during the whole process. In order to take into account the influence of the substrate, one must solve the energy equation for the substrate and for the billet respectively. The model includes a constant thermal conductivity and specific heat within the substrate. The two domains of the computation are combined by the interfacial heat flux.

Boundary and initial conditions for the problem of transient heat conduction are (see Fig. 2) the heat flux over the fixed and moving surface of the billet, and the initial temperature of the substrate.

The heat flux over the surface is driven by convection, radiation, conduction, and also by the incoming enthalpy of the impinging droplets in the spray.

The heat flux $\dot{q}_\alpha$ from the surface of the billet due to gas convection is determined by

$$\dot{q}_\alpha = \alpha(T_w - T_u) \tag{12}$$

with the temperature difference between the ambient air T_u and the local temperature of the surface T_w, and the convective heat transfer coefficient α. The heat flux from the surface to the environment by thermal radiation is [23]:

$$\dot{q}_\varepsilon = \sigma\varepsilon\big(T_w^4 - T_{\text{ch}}^4\big) \tag{13}$$

where T_w is the temperature of the surface of the billet, T_{ch} is the temperature of the spray chamber wall, ε is

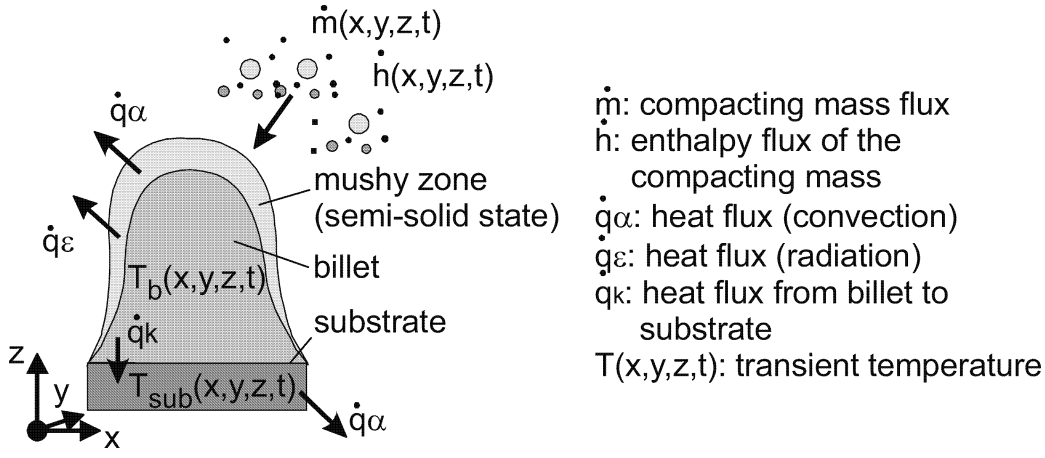

Fig. 2. Boundary conditions for the energy balance.

the emissivity, and σ is the Stefan–Boltzmann constant. In the spray forming process, the heat transfer between the billet and the substrate is often decreased by an incomplete interfacial contact, and by porosities in the contact zone (deposit/substrate). This heat flux can be written as

$$\dot{q}_k = k(T_b - T_{\text{sub}}) \tag{14}$$

where k is the heat transfer coefficient at the substrate-billet interface, T_b is the temperature at the bottom of the billet, and T_{sub} is the temperature at the upper surface of the substrate. The coefficient k has to be determined from post-analysis [24] of spray formed products. For numerical solution of the governing equation, the boundary conditions must be rewritten with the Kirchhoff transformed temperature, thereby linearizing non-linear boundary conditions.

A finite-difference method is used to discretize the governing equation. The resulting numerical discretization of Eq. (11) is based on implicit time integration. For the diffusion transport term, a non-conservative discretization is used. The resulting implicit system of equations is solved by an iterative method (successive over-relaxation).

2.2. Grid generation and billet growth

In the growing domain during the spray process, a fixed, non-orthogonal boundary-fitted coordinate system is used for the grid generation. The generated grid distribution is based on the transient shape of the billet. Fig. 3 shows an outline of the grid used and the final shape of an experimentally produced billet. The transient surface and geometry of the billet is calculated by means of a geometry simulation program [18]. The geometry model considers the mass flux distribution within the spray (based on measurements), the scanning motion of the atomizer, the rotation of the substrate, the withdrawal motion of the substrate and some other geometrical parameters (distance, eccentricity, . . .). In Table 1, important parameters are listed. By varying the sticking efficiency, the calculated billet geometry and the geometry of the produced billet are adjusted. However, a difference remains between the calculated and the actual spray formed billet shape (Fig. 3).

A local grid refinement is necessary as the billet height increases. The grid refinement and rearrangement allows for appropriate and continuous spreading of the grid in the lateral direction over the whole billet height while maintaining sufficient resolution at the outer edge of the domain. The transient heat conduction problem with a phase change is solved on the shown non-orthogonal grid by making a coordinate transformation in the governing equation from cylindrical coordinates Eq. (11) into the non-orthogonal, boundary fitted coordinate system of the grid [25].

Growth of the billet and the heat flux on its surface are modeled by subsequently adding thin layers on the time-dependent billet geometry. Therefore, after each time step a new layer of grid cells is added to the domain. The geometry, liquid fraction and temperature of these new grid

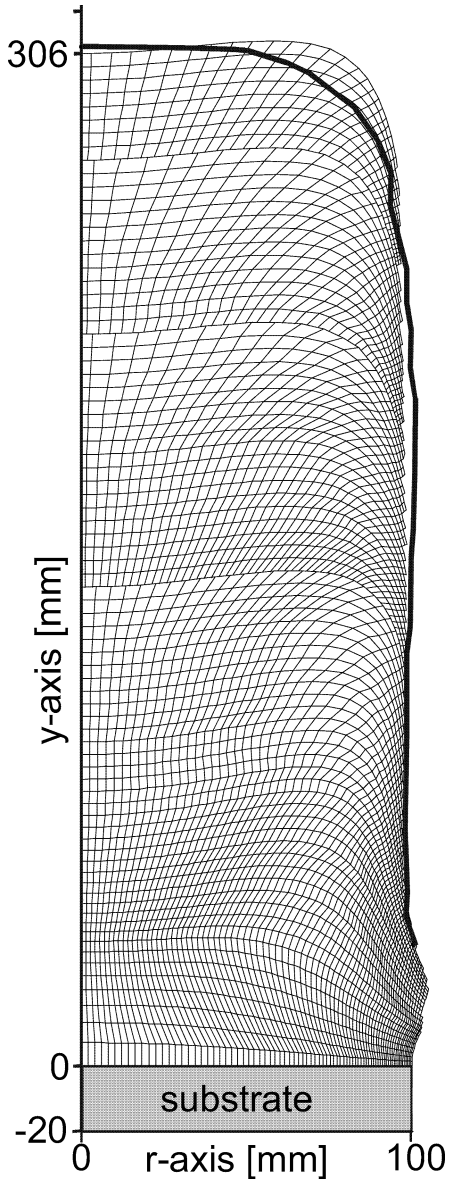

Fig. 3. Used grid for simulation of the billet (solid line = experimental result).

Table 1
Process parameters

melt superheat [K]	250
gas to metal ratio (GMR)	0.72
metal flow rate [kg·s^{-1}]	0.32
spraying distance [mm]	500
angle between the axis of the spray cone and the substrate [degree]	30
scanning angle of the spray cone [degree]	3.6
eccentricity [mm]	40
scanning frequency [Hz]	15.2
spray time [s]	360
withdrawal velocity of the substrate [mm·s^{-1}]	0.85
rotation frequency of the substrate [Hz]	2.45
initial temperature of the substrate [K]	291

cells correspond to the mass flux and thermal conditions within the impacting spray. The impacting local mass vary with the radius of the billets top and is calculated by the geometry simulation program. For a given time step width, the geometry model predicts the local thickness of each added grid layer. The local liquid fraction, temperature, and mass flux determine the enthalpy flux onto the top of the billet. The liquid fraction and temperature within each new grid cell is determined, e.g., from experiments [27] or numerical simulations [8,9,24]. During addition of a new grid layer, a pronounced temperature gradient between the previous billet surface and the new layer may exist. The billet surface cools down till the next hot layer is added. To obtain a good resolution and improve the numerical accuracy of these temperature gradients, the new added layer consists of several subgrid layers at each time step. For the present computation, each layer shown in Fig. 3 represents four subgrid layers (each shown grid cell represents 16 cells). After addition of a grid layer, the energy equation is solved with the above described boundary conditions for the present time step. Due to the scanning motion of the spray and the rotation of the billet each point on the billets top is hit by an oscillating mass flux. This unsteady behaviour is not taken into account for the computations, but is averaged over each 360° turn of the billet. Therefore, the used time step width has to be small. A decreased time step increases the computational time as the number of grid cells in the domain increases, but will more accurately describe the thermal conditions on the surface of the billet.

3. Experimental procedure

Temperature measurements have been performed within spray forming of billets in the rotating substrate plate and in the billet by thermocouples of type *K* (NiCr–Ni). The thermocouples are positioned at various radial distances from the rotational axis at different heights above the substrate from below and within the substrate. The experimental set up for temperature measurements is shown in Fig. 4. The drive of the substrate plate is done through a hollow shaft. Through this shaft the signals from the thermocouples are transferred to the data recorder, which is mounted to the rotating shaft. The measured signals are stored and can be recalled after the spray forming process. For protection of the data logger and the transmission line gas cooling is used. After the experiment the thermocouples are enclosed within the billet and must be renewed for each experiment.

Possible disturbances within this kind of temperature measurement are due to previously impinging droplets (before total embedding of the thermocouple) and the possible formation of gas pores around the thermocouples. This effects are of minor importance, which has been justified by two observations. First, from in-process video recordings, up to 40 seconds spray time no disturbance of the billet growth process due to the presence of the thermocouple

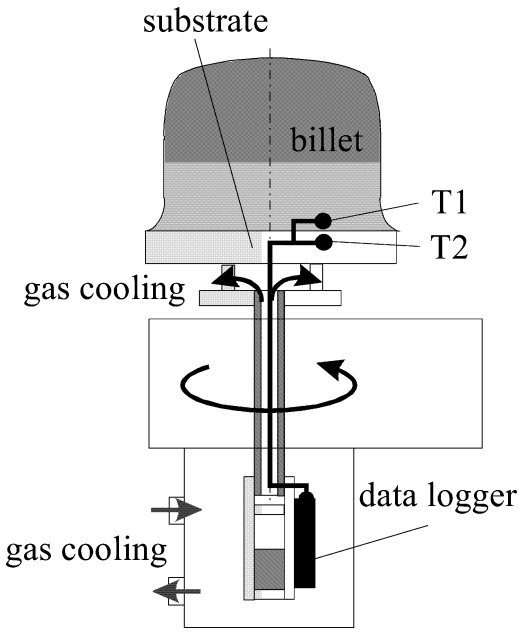

Fig. 4. Experimental set up for temperature measurements.

has been observed in the shape of the billet. Second, from ex-post microscopic analysis of the area close to a thermocouple, no distinct pore formation could be found. At the beginning of the spray forming experiment the thermocouples must be heated up by the impacting particles. Due to the small thermal mass of the thermocouples this influence can be neglected after a few seconds. In addition, due to the high thermal conductivity of CuSn6 it can be assumed that for later times (>40 seconds) the disturbing influence on the temperature field in the billet by the thermocouples may also be neglected. In total it is expected that the temperature measurement signal from the thermocouples may lag behind the real temperature distribution, but not more than a few seconds, which is not important for the data discussion in the present investigation.

4. Results

4.1. Temperature measurements

The most important process parameters for the spray forming experiments with CuSn6 for temperature measurements are listed in Table 1. In the first 40 seconds of the experiment the substrate plate distance to the atomizer remains constant as the substrate is not withdrawn downwards in this time.

Measured temperatures are plotted versus time in Fig. 5 together with the locations of the different measurement points. In point T1 it must be noticed that it takes some time till this thermocouple is enclosed by the growing billet.

In the beginning of the spray experiment the melt is sprayed directly onto the thermocouples, which are positioned above the substrate. According to this in the first

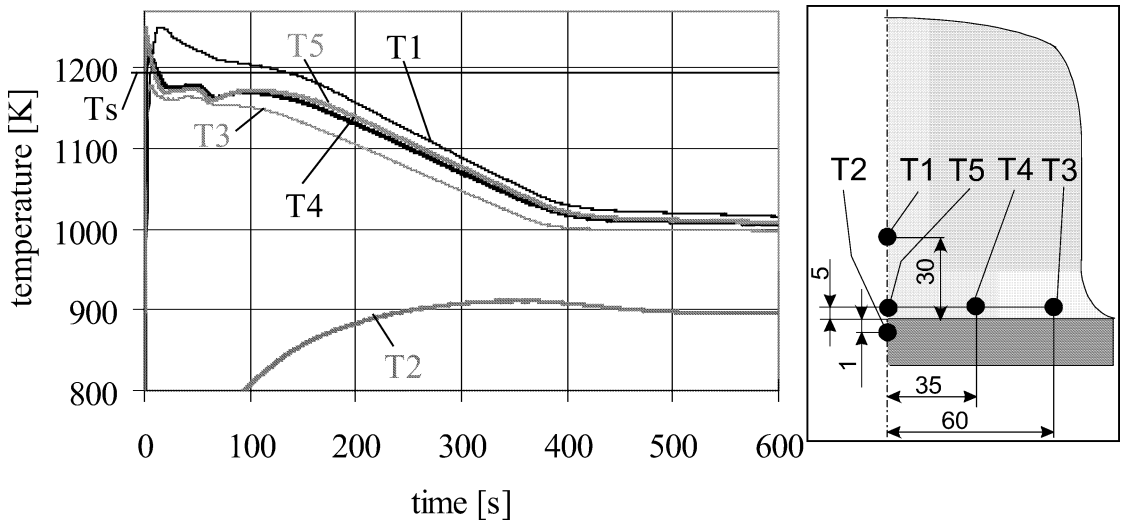

Fig. 5. Measured temperatures and locations of the measurement points within the billet and substrate.

Table 2
Used material properties for the simulation [28,30–33]

Material properties	Billet	Substrate
material	CuSn6 (2.1020)	low carbon steel
liquidus temperature [K]	1325	
solidus temperature [K]	1189	
latent heat of solidification [kJ·kg^{-1}]	199.971	
average thermal conductivity [W·m^{-1}·K^{-1}]	153	46
	(1023 K–1189 K)	(293 K–923 K)
density [kg·m^{-3}]	8484	7737
	(Cu, 1173 K)	(293 K–923 K)
average specific heat [J·kg^{-1}·K^{-1}]	478	635
	(Cu, 1023 K–1301 K)	(293 K–923 K)

seconds a high temperature may be measured. Measured maximum temperatures within the billet are above solidus temperature T_s of the alloy (Table 2).

Due to the direct contact with the cold substrate a lot of heat is transferred from the lowest part of the billet into the substrate. This can be seen in Fig. 5 by the strong increase of the substrate temperature (initial temperature of the substrate is 291 K) and the drop of the temperature within the bottom of the billet (T3–T5) during the first few seconds. After this short time period the increasing temperature within the substrate leads to a strong decrease of the cooling rate in the billet. With increasing time the distance between the sensor locations (T1, T3, T4, T5) and the top of the billet increases as the surface of the billet rises. Thereby the heat flux from the billet surface to the lowest part decreases and the loss of heat from the surface increases. This leads to a temperature decrease in the base of the billet. With growing distance from the central axis, the temperature within the lowest part of the billet is reduced (T5 to T3).

Because of the high thermal conductivity of the copper alloy (Table 2) the radial temperature gradient is relatively low. Following the spraying time period, the billet is removed from the gas flow of the atomizer (after 360 s). Due to this removal, the convective heat transfer on the billet surface distinctly diminishes. This can be seen from the slow cooling rate of the billets lowest part after the spraying time period.

A comparison between sensor locations T1 and T5 indicates a decreasing temperature within the billet in the direction towards the substrate plate.

The temperature of the substrate increases during the spraying time and afterwards decreases slowly during the cooling period. Thereby, the temperature level of the billets base is not reached. This effect is due to the influence of the heat transfer coefficient k from the billet to the substrate Eq. (14), and the heat transfer rate from the substrate plate to the environment. The bottom of the plate has to be cooled to prevent the thermocouple transmission lines from damage due to overheating (Fig. 4).

4.2. Simulation of the billet thermal history

Several process and material parameters as well as boundary conditions need to be described as part of the computation. The material properties used in the simulation are listed in Table 2. A parameter variation on the boundary conditions is executed based on variations of the standard

Table 3
Standard boundary conditions for the computation

Parameter	Spray time	Cooling time
convective heat transfer coefficient/billet surface [W·m^{-2}·K^{-1}]	280	10
average liquid fraction of the spray	0.5	
average temperature of the spray [K]	1295	
temperature of the ambient air	523	523
and the spray chamber [K]		
emissivity/billet surface	0.18	0.18
convective heat transfer coefficient/substrate bottom [W·m^{-2}·K^{-1}]	250	250
initial temperature of the substrate [K]	303	
heat transfer coefficient at the substrate billet interface [W·m^{-2}·K^{-1}]	1000	1000
time steps till a new layer is added [s]	4.67	

process conditions listed in Table 3. Determination of the thermal conditions (temperature, liquid fraction) of the impacting spray is difficult. Some authors investigate these thermal conditions by numerical models [7,9,10,15], other authors describe different measurement techniques [12,26, 27]. However, the enthalpy flux depends on a lot of process and material parameters and a wide range of results can be found. For that reason a parameter variation based on temperature measurements within the billet and based on frequently used boundary conditions has been carried out. Estimation of ambient gas temperature is based on measurements within the spray chamber, the gas temperature is assumed to be constant. The convective heat transfer coefficient at the billets surface and the thermal state of the impacting spray for the standard case was estimated by adjusting the calculated temperatures to the measured ones. The adjustment is based on previous determinations of heat transfer coefficients [4] and the fact, that the chosen experiment was realized with relatively hot spray conditions. The gas to metal ratio was relatively low ($GMR = 0.72$) and therefore the specific enthalpy of the spray relatively high [12,24,27]. For that reasons the chosen liquid fraction for the standard case was taken to $f_l = 0.5$. The liquid fraction within the spray is assumed to be constant over the billets radius. For the emissivity value of the billet surface, literature data for copper are used [28,29], and the heat transfer coefficient at the substrate billet interface was based on available data for similar solidification processes [4,15, 24]. The initial temperature of the substrate was taken from thermocouple measurements.

For most computations averaged material properties over the relevant temperature range (Table 2) are used. Only the computation with standard boundary conditions is performed including the full temperature dependency of thermal conductivity and specific heat. A test computation with and without respect to the temperature dependency of the material properties has shown very similar results, where the relative temperature change is lower than 0.6%. Therefore, for reduction of computational time and without loss of accuracy, for all further computations only temperature averaged material properties are used. The temperature range for averaging the material properties is indicated in Table 2 (in brackets). The substrate material is low carbon steel. The temperature averaged material properties of the substrate are derived from interpolated data [30]. Some material properties of CuSn6 alloy (especially in the solidification temperature interval) are not well known. Therefore, the temperature dependency of specific heat and density are derived from data of pure copper [30]. Especially the thermal conductivity strongly depends on the composition of the copper alloy. Therefore, the temperature dependent thermal conductivity is extrapolated by using given data of CuSn-alloys at a similar tin content [28,30–33].

The governing equation Eq. (11) is given in terms of two variables: the temperature field and the local liquid fraction are unknown. In the following, it will be assumed that the liquid fraction is only a function of the temperature:

$$f_l = F\big(T\{t\}\big) \tag{15}$$

The dependency of liquid fraction versus temperature mainly depends on the alloy composition and the solidification rate [34]. Especially in spray forming, the cooling rate may be too high to allow substantial diffusion in the solid phase. This may lead to a modified dependency of liquid fraction versus temperature. However, here equilibrium solidification is assumed and therefore the CuSn equilibrium phase diagram is used to determine the basic function [28], shown in Fig. 6. This curve causes a non-linear source term in the matrix form of the discretized equations. Therefore, the curve is approximated by a piecewise linear function (polygons) resulting in a piecewise linearisation of the equation system. In the following, simulation results based on the above mentioned models and boundary conditions are presented.

4.2.1. Thermal history with adapted boundary conditions

The simulation results for temperature distributions at distinct locations, illustrated in Fig. 7 for the standard boundary conditions, are in agreement with the measured temperatures shown in Fig. 5. The used standard boundary conditions within the simulations have been adapted to these measurements. Fig. 8 shows the comparison between measurement and calculation results. The measured and computed temperatures are compared at the same time. For measurement position T1 the temperature data after the

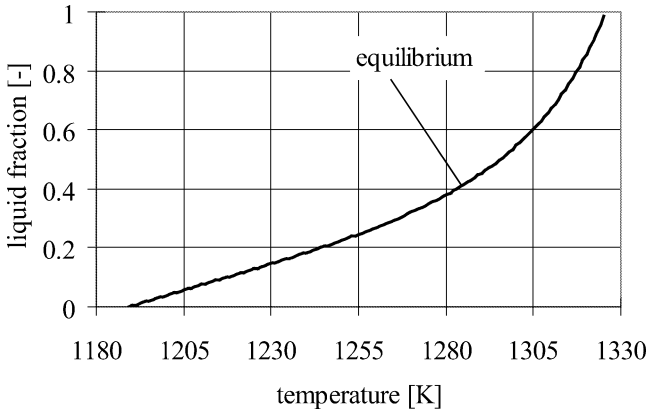

Fig. 6. Liquid fraction versus temperature function of CuSn6 determined from equilibrium phase diagram [28].

first 40 s of the experiment and for the other positions (T3–T5) after 5 s are plotted. This considers that it takes some time till the thermocouple T1 is enclosed by the growing billet and the thermocouples T3–T5 will reach the temperature of the impacting particles. Some differences between measured and calculated results can be noticed at the highest temperatures. The maximum temperature deviation is 50 K. After 40 s, the temperatures at measurement points T3–T5 are below 1190 K (Fig. 7) and the temperature deviation is always lower than 25 K. The maximum temperature deviation at the measurement position within the substrate (T2) is 70 K. This deviations depend on the assumed boundary conditions. The used set of standard boundary conditions are adapted to the measurements with consideration of frequently used data. However, still a large number of free parameters remain.

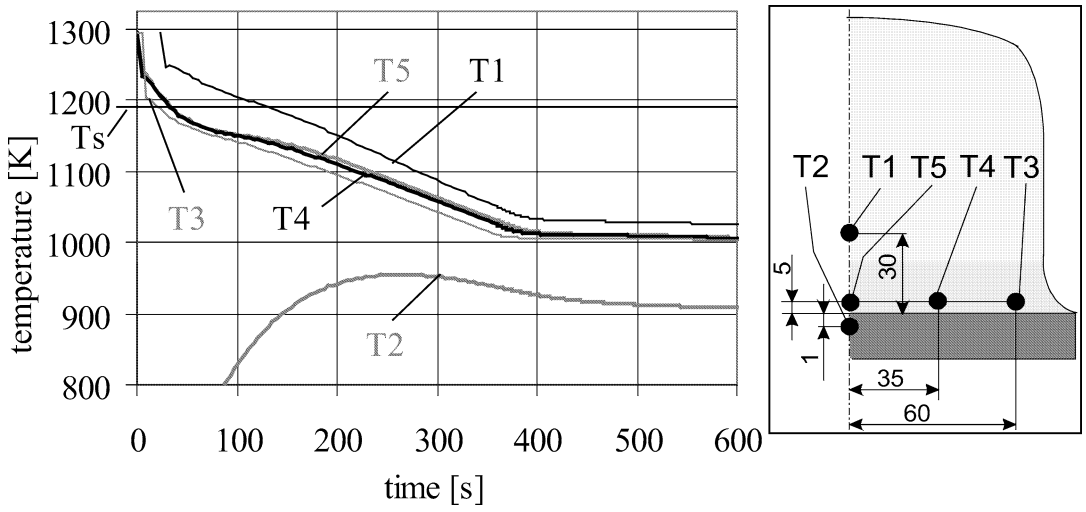

Fig. 7. Computed temperature profiles with standard boundary conditions and locations of the different positions within the billet.

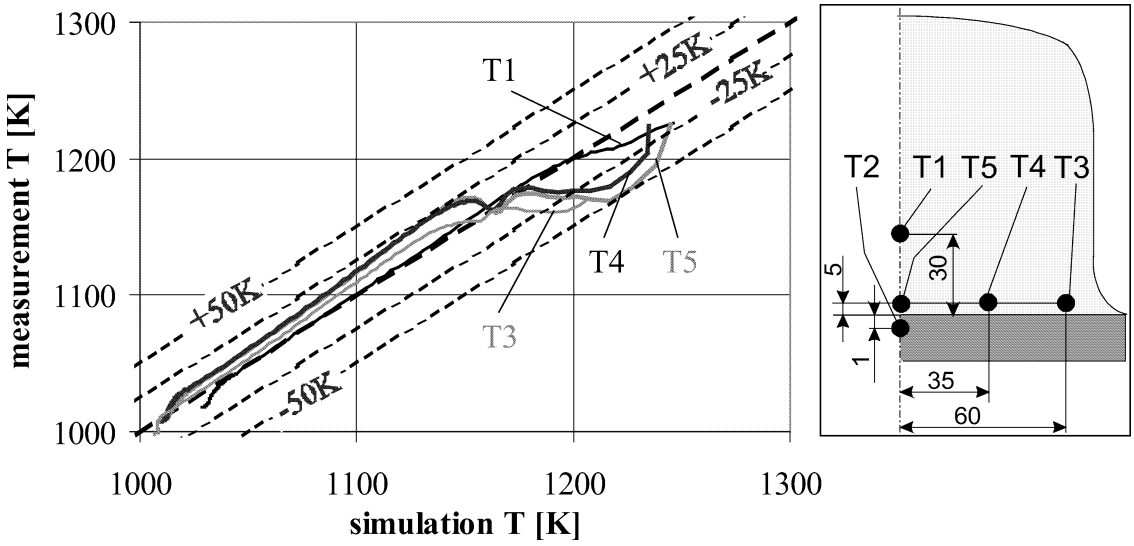

Fig. 8. Extend of agreement between measured and calculated temperatures.

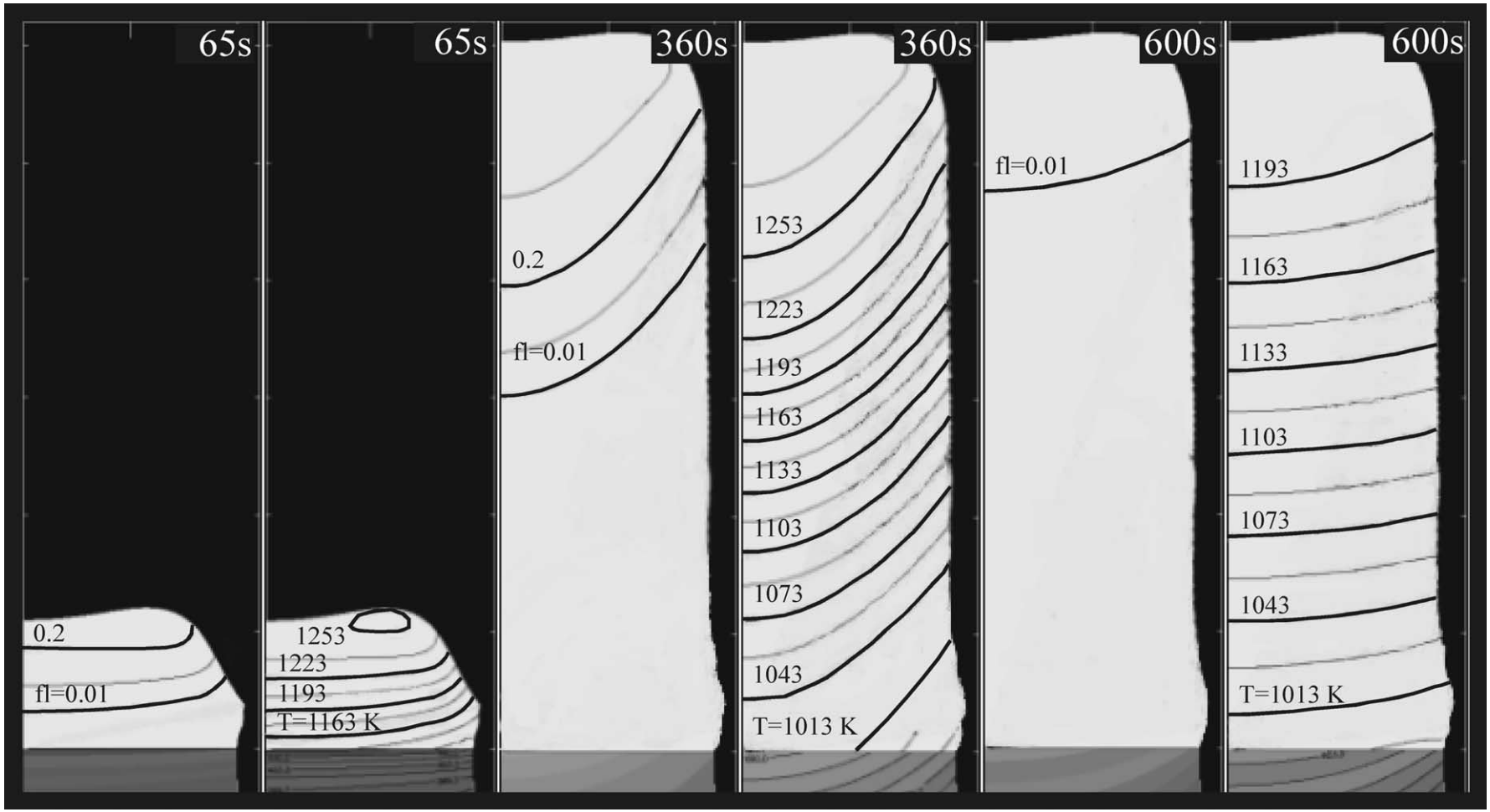

Fig. 9. Temperature field (left) and local liquid fraction (right) in the billet—calculated with the standard conditions—at different times.

The overall temperature and local liquid fraction distribution in the billet at different times are illustrated in Fig. 9. Until the end of the spraying period (360 s), the billets height increases. During the whole spraying period the calculated liquid fraction in the billet is high. This can be explained by the chosen standard conditions—particularly by the high liquid fraction in the impacting spray ($f_l = 0.5$).

After the spraying period, the billet cools down slowly and the residual liquid in the mushy zone solidifies. Because of the high thermal conductivity of the material the temperature gradient from billets top to base as well as along the radius is relatively low. Along the radius this is especially valid after the spraying period. During this period the convective heat transfer coefficient is low and therefore, a more constant radial temperature distribution is expected (lower Biot number). The highest temperature gradients are located at the bottom during the beginning of the process (Fig. 9, 65 s). In the upper part of the billet the temperature gradients are lowest because of the great amount of enthalpy which is contained in the mushy zone in form of the latent heat of solidification (Fig. 9, 360 s).

Fig. 10 shows the calculated variation of temperature with time for the standard conditions on the centre line of the billet in different distances to the substrate plate. During the spray process the billet height increases and the billet top reaches the different measurement positions at different times. From billet top to bottom the temperature within the billet decreases. The highest cooling rate is at the billet base in the beginning of the spraying process, where the spray cone hits the cool substrate plate. The rapid change of the cooling rate at top of the billet after 650 seconds is due to the termination of the solidification process at the billet surface.

The boundary and initial conditions which mainly influence the thermal history within the billet can be subdivided into free and restricted process parameters. The free parameters are those which can be changed without influencing other boundary conditions. One of the most important of these parameters is the heat flux across the billets surface after the end of the spray period. Here, the gas flow conditions around the billet (flow velocity, flow direction) or the temperature of the gas may be directly controlled. Furthermore, the initial temperature and bottom cooling of the substrate can be freely modified as well as the material of the substrate. The spray enthalpy entering the top of the billet during the spraying process, and the heat flow from the billets surface to the gas phase by convection (during the spraying period) behave in a different way than the parameters listed before. These parameters are directly combined to each other. Both heat fluxes are influenced by the atomization parameters and the melt overheating temperature. Thus, the local mass flux and the enthalpy of the particles in the spray are influenced by the GMR. At the same time, the heat is transferred to the gas and the gas velocity in the spray changes. The geometry of the billet may change by varying the substrate motion and is also influenced by the local particle sticking efficiency. The particle sticking efficiency mainly depends on the temperature of the billet surface and the spray conditions (mass flux distribution, liquid fraction within the particles) [35]. The heat transfer process at the substrate/billet interface is not controllable as well. It depends on the surface quality of the substrate, the thermal conditions within the substrate, the condition of the initially impinging spray, and on the sprayed material.

For investigation of the influence of different fundamental process parameters on the spray forming process and the thermal history within a billet, a parameter variation for boundary conditions is executed based on the standard conditions discussed above. This parameter study analyze the qualitative influence of a deviation of the estimated standard boundary conditions on the calculated thermal history of the billet.

4.2.2. Influence of the specific enthalpy of the impacting spray

In Fig. 11 the total liquid mass in the billet versus time is shown for different liquid fractions in the spray. With increasing liquid fraction the results show a strong increase of the maximum melt mass within the billet. Mingard et al. [26] already recommended to minimize the liquid fraction in a sprayform to minimize macro-segregation. Furthermore, a

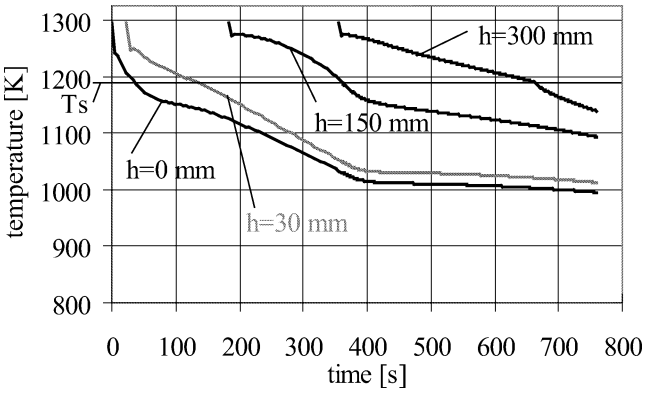

Fig. 10. Computed temperature profiles with standard boundary conditions on the billet centre line at different distances to the substrate.

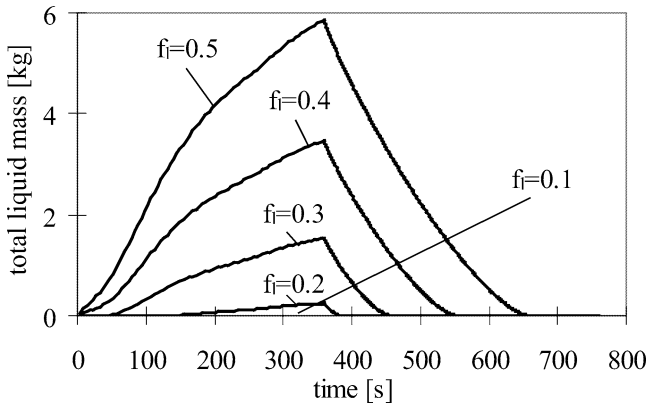

Fig. 11. Total liquid mass within the billet versus time for different liquid fractions within the spray.

pronounced influence of the liquid fraction on the porosity within the billet is proved. A too low as well as a too high liquid fraction may increase the porosity [4,6,12]. The amount of liquid within the spray has to optimized for each alloy with respect to the desired product quality. Only for an estimated spray liquid fraction of $f_l = 0.1$ and below, the mushy zone is thin and the melt in the uppermost grid layer of the computation solidifies already before the next layer is added. The thickness of the mushy layer in this case is smaller than the vertical grid resolution. Fig. 11 shows the liquid mass just before the next layer is added and therefore, the presented melt mass in the billet is vanishing during the whole computation for $f_l = 0.1$. Nevertheless, just after each addition of a new layer a small semi-liquid area exists. The remaining liquid in the spray solidifies very fast and the development of interstitial porosities may be expected [4,6]. Up to the end of the spraying period at 360 seconds, the total melt mass increases steadily for a liquid fraction of 0.2 to 0.5. In these cases the mushy zone thickness steadily increases. The thermal conditions within the billets top are changing during the whole spraying process. Hence, the resulting material properties will vary with the billets height. After the end of the spraying period, the remaining melt within the billet solidifies. The length of the time period until solidification is finished depends on the quantity of the remaining melt in the mushy zone.

4.2.3. Influence of the heat loss during the spray process

For the simulation results illustrated in Fig. 12 the convective heat transfer coefficient α at the billet surface used during the spraying period has been changed. With increasing convective heat transfer coefficients the total amount of liquid mass in the billet decreases. The computations for convective heat transfer coefficients of 400 $W \cdot m^{-2} \cdot K^{-1}$ and 500 $W \cdot m^{-2} \cdot K^{-1}$ respectively show a relatively low change of the melt mass in the mushy zone during the spray time. A decrease of the convective heat transfer coefficient leads to a reduction of the heat flux to the environment and therefore, the total enthalpy within the billet increases. Furthermore, the results of the model show that the temporal change of the liquid mass in the billet (and with this the mushy zone thickness) can be controlled by varying the convective heat transfer coefficient. An almost identical effect on the thermal history can be obtained by changing the temperature of the ambient gas Eq. (12). The computations indicate that the temporal extent of the mushy zone is highly influenced by the liquid fraction in the spray cone and the gas flux.

The initial temperature of the substrate plate (controlled by preheating of the substrate) influences the heat flux at the billets base in the initial phase of the spray forming process. This correlation is mainly important for the production of spray formed plates and strips which are relatively thin. The influence of the initial substrate temperature on the billet thermal history at the beginning of the process is shown in Fig. 13 by illustrating the total liquid mass in the billet. With increasing initial temperature of the substrate plate the total melt mass within the billet rises slightly. This occurs mainly at the beginning of the spraying process.

4.2.4. Influence of the heat loss during the cooling period

During the cooling period some parameters may be easily controlled. These are the convective heat transfer coefficient and the temperature of the environment. By increasing the convective heat transfer coefficient at the billet surface (during the cooling period) the solidification time of the remaining melt in the cooling period decreases as shown in Fig. 14. Besides this correlation, the temperature field and the mushy zone are changing by varying the cooling conditions. This is shown in Fig. 15 for $\alpha = 600$ $W \cdot m^{-2} \cdot K^{-1}$. In this figure, the calculated mushy zone and the temperature distribution in the billet 60 seconds after the end of the spraying period are illustrated. Within the top of the billet a "hot-spot" is formed. Because of the high heat loss across the billets surface the melt at the upper part rapidly solidifies and a semi-solid area is enclosed. In this case the material shrinkage during cooling may cause hot cracking [16]. Furthermore, at the billets top a substantial increase of the temperature gradients in radial direction occurs. By reducing the heat transfer rate in this cooling period, the hot spot risk may be avoided and a more regular

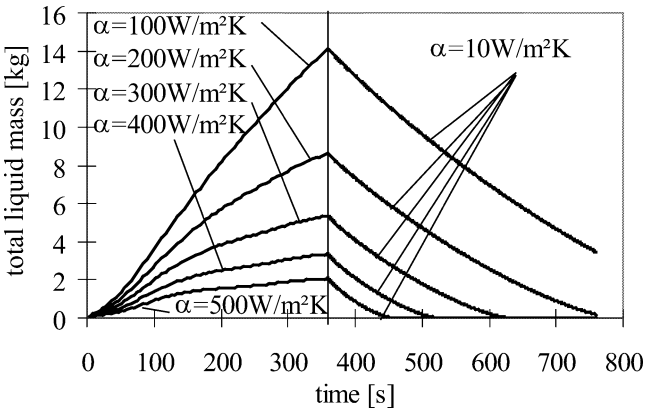

Fig. 12. Total liquid mass within the billet versus time for different heat transfer coefficients at the billet surface during the spray phase.

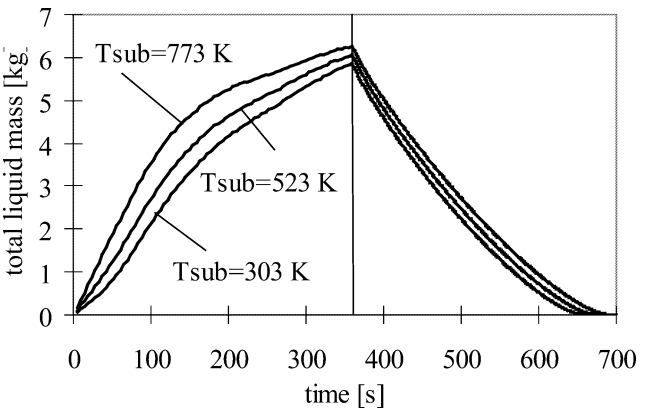

Fig. 13. Total liquid mass within the billet versus time for different initial substrate temperatures.

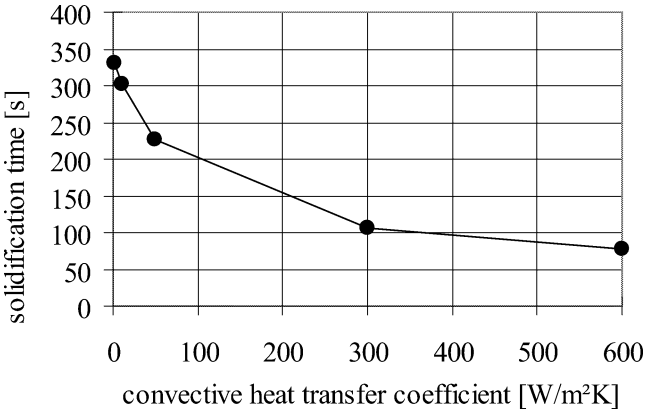

Fig. 14. Solidification time of the remaining melt within the billet versus convective heat transfer coefficient during the cooling period.

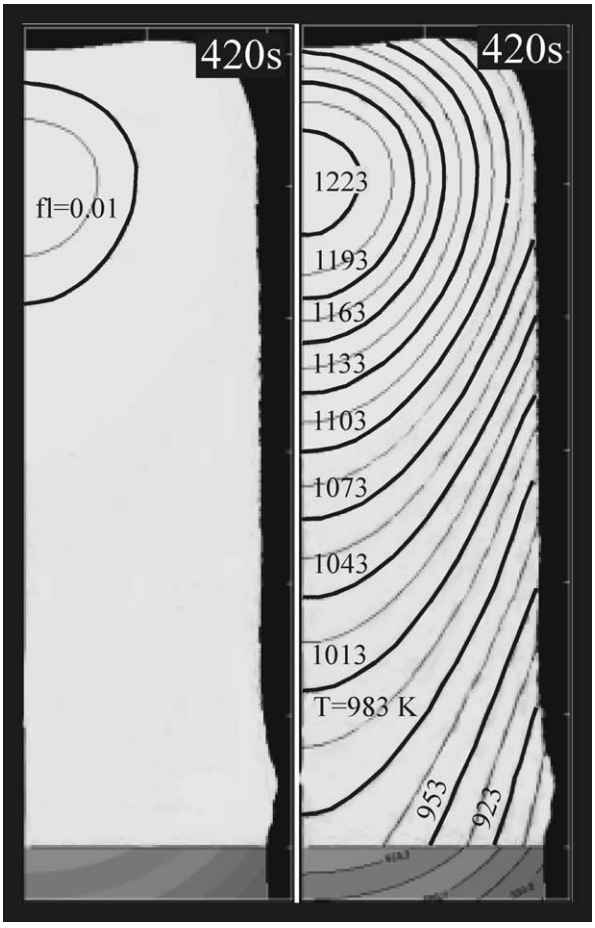

Fig. 15. Temperature field and local liquid fraction in the billet calculated with a high cooling rate ($\alpha = 600$ W·m^{-2}·K^{-1}) after the spray time.

temperature profile at the billets top is realized as shown in Fig. 9 (600 s).

4.2.5. Influence of the heat transfer coefficient at the substrate/billet interface

The heat transfer coefficient at the substrate/billet interface cannot be influenced directly. In combination with the

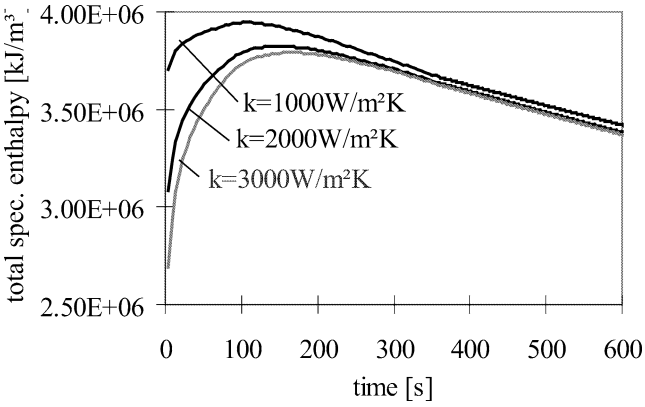

Fig. 16. Total enthalpy of the billet divided by the time depending volume versus time. Influence of the heat transition coefficient at the substrate/billet interface.

temperature of the substrate it determines the heat flux from the billet to the substrate mainly in the beginning of the spraying period. This can be illustrated by an integral energy balance in the billet. Fig. 16 shows the total enthalpy Eq. (2) divided by the actual volume of the billet versus time. For this computation a constant specific heat value (Table 2) is used and the reference temperature used is $T_{\text{ref}} = 273.15$ K. An increasing heat transfer between the billet and the substrate ($k = 1000$–3000 W·m^{-2}·K^{-1}) causes a decrease of the volumetric specific enthalpy at the beginning of the process. During the spraying period the temperature of the substrate increases and the heat flux decreases. Thereby, the influence of different transition coefficients decreases with process time. At first, the specific enthalpy per unit volume increases with spraying time. During the first seconds the impacting mass contains a substantially higher total enthalpy than within the billet because of the relatively high heat loss across the bottom of the billet. With increasing height of the billet, the free surface of the billet and also the heat flux across the surface increases. In that part of the plot where the volumetric specific enthalpy reaches a maximum, the incoming enthalpy of the impacting mass and the heat loss across the surface are balanced. With increasing time in the spray period, the incoming energy becomes smaller than the heat loss over the growing surface and the volumetric specific enthalpy slowly decreases.

4.2.6. Comparison of the influence of the varied boundary conditions

The parameter variation shows a pronounced influence of the spray liquid fraction and the heat transfer coefficient on the thermal history of the billet. The temperature history within the billet has an effect on the microstructure and the material properties of the sprayformed product. For that reason, the influence of these important parameters on the time dependent temperature—at two different locations within the billet—is shown in Figs. 17 and 18. Fig. 17 illustrates the influence of the parameters on the axis of the billet at a height of 150 mm (midth of the billet). After 182 s

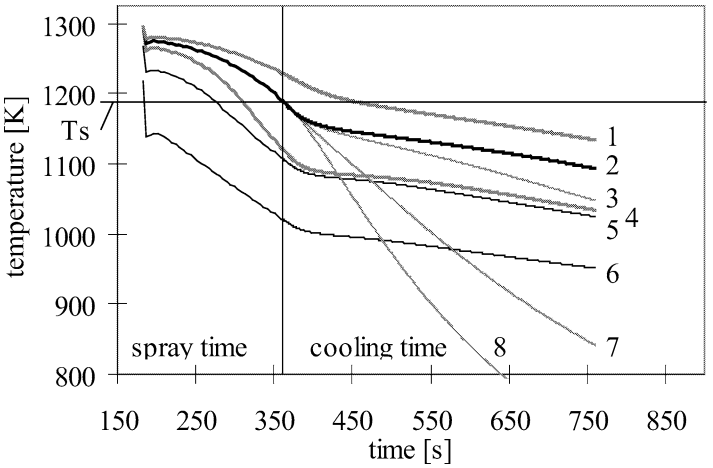

nr.	fl	α1	α2
1	0.5	200	10
2	0.5	280	10
3	0.5	280	50
4	0.5	400	10
5	0.3	280	10
6	0.1	280	10
7	0.5	280	300
8	0.5	280	600

Fig. 17. Temperature on the axis of the billet at a height of 150 mm versus process time for different boundary conditions (fl: liquid fraction [/], $\alpha 1$: heat transfer coefficient during spray time [$W \cdot m^{-2} \cdot K^{-1}$], $\alpha 2$: heat transfer coefficient during cooling time [$W \cdot m^{-2} \cdot K^{-1}$]).

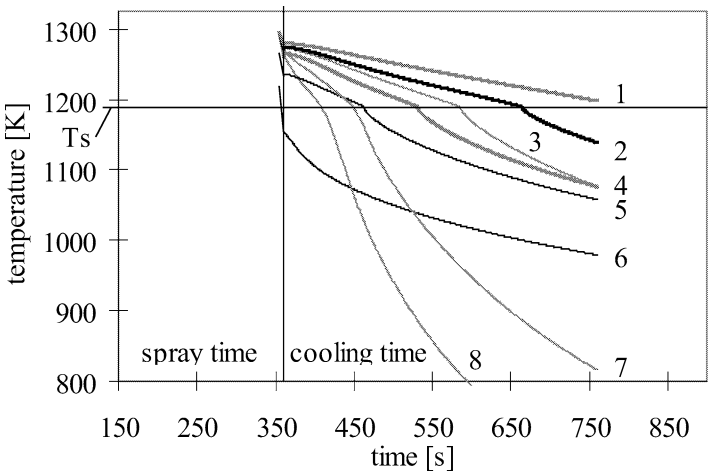

nr.	fl	α1	α2
1	0.5	200	10
2	0.5	280	10
3	0.5	280	50
4	0.5	400	10
5	0.3	280	10
6	0.1	280	10
7	0.5	280	300
8	0.5	280	600

Fig. 18. Temperature on the axis of the billet at a height of 300 mm versus process time for different boundary conditions (fl: liquid fraction [/], $\alpha 1$: heat transfer coefficient during spray time [$W \cdot m^{-2} \cdot K^{-1}$], $\alpha 2$: heat transfer coefficient during cooling time [$W \cdot m^{-2} \cdot K^{-1}$]).

the billets reaches the investigated point and the temperature is plotted versus time. Directly after addition of the new grid layer, the temperature drops very fast, because the surface of the billet is colder than the temperature of the new added layer. A great amount of the liquid solidifies during the first seconds. With decreasing liquid fraction (Fig. 17; no.: 2, 5, 6) within the spray (decreasing enthalpy) the temperature jump increases. If the enthalpy within the spray is low, the new layer solidifies before the next layer is added. In this case the mushy zone exists only during a very short time and within a very limited area. This may cause the development of porous layers within the billet, caused by insufficient liquid to feed the interstices between deposited droplets [6, 12]. In contrast, a too high amount of liquid within the top of the billet may intensify another type of porosity, which is caused by gas entrapment and solidification shrinkage [6]. Furthermore, the figure shows a general increase of the temperature with a higher amount of enthalpy within the spray. Due to the high latent heat contents a variation of the liquid fraction within the spray shows a pronounced influence on the temperature level within the billet. The cooling rate within the billet can be adjusted by the heat transfer coefficient. But only the heat transfer coefficient during the cooling period can be easily varied over a wide range. The heat transfer coefficient during the spray period (Fig. 17; no.: 1, 2, 4) has a relatively small effect on the sharp temperature decrease after adding a new layer. With increasing heat transfer coefficient the liquid fraction and the temperature reaches a lower level after the spray period. The cooling rate after the spray period (Fig. 17; no.: 2, 3, 7, 8) can be easily controlled by the ambient gas flow or the gas temperature. With these process conditions, the cooling rate can be changed within a wide range.

A comparison between Figs. 17 and 18 shows the local dependency of the thermal history in the billet. Fig. 18 illustrates the temperature in the billet at a height of 300 mm (top of the billet) versus the processing time. After 355 s the billets height reaches the investigated point and after 360 s the spray period ends. For that reason the liquid fraction (Fig. 18; no.: 2, 5, 6) and the heat transfer coefficient

during the cooling period (Fig. 18; no.: 2, 3, 7, 8) are the most important parameters. Completion of the solidification process after the spraying period is clearly marked by a sharp increase of the cooling rate.

5. Summary and conclusions

In the present study, modeling fundamentals for the thermal simulation of spray formed billets are described. It is shown, that by means of the derived simulation program the thermal simulation of real billet geometries is practicable. Simulation results are fitted to temperature measurements in a growing and rotating billet. Within the set of used standard boundary conditions an agreement between measured and computed temperatures is achieved. A parameter variation is executed to discussing the qualitative influence of different process parameters and the used boundary conditions on the computed thermal history and solidification within a CuSn6 (2.1020) billet. In the spray forming process, the cooling conditions after the spray period can be easily controlled by changing the temperature of the ambient gas or the gas flow conditions around the billet. Therefore, the cooling rate of the billet as well as the solidification time of the remaining melt can be influenced. Too high cooling rates may cause the development of a hot spot and due to this some risk of hot cracking. The control of the thermal history of the billet during the spraying period is more difficult, because the important parameters are coupled. For example, the local energy and material flux into the billet, the heat flux from the surface to the environment, and the geometry of the billet are affected by the type of atomizer, the spraying distance, the GMR, and the substrate movement. The computations show a pronounced dependency of the total liquid mass within the billet and the development of a mushy zone on the liquid fraction within the spray, the convective heat transfer coefficient at the billet surface, and the temperature of the ambient gas. These parameters have to be exactly adjusted to each other to achieve constant and reproducible thermal conditions within the mushy zone during the whole spray period. Also the enthalpy of the spray and the cooling conditions during the spray process mainly determine the solidification and cooling rate on top of the billet and therefore the porosity of the billet. Depending on the process conditions a wide range of solidification rates—complete solidification within a few seconds or development of a pronounced mushy zone—are possible.

Acknowledgement

The authors gratefully acknowledge the support of this project by the Deutsche Forschungsgemeinschaft (DFG) within the Collaborative Research Centre 372 “Spray Forming” at the University Bremen, Germany.

References

[1] K. Hummert, PEAK Werkstoff GmbH, Velbert: PM-Hochleistungsaluminium im industriellen Maßstab, in: K. Bauckhage, V. Uhlenwinkel (Eds.), in: Kolloquium des SFB 372, Vol. 4, Universität Bremen, 1999, pp. 21–44, ISBN 3-88722-440-X.

[2] H.R. Müller, A.G. Wieland-Werke, Ulm: Eigenschaften und Einsatzpotential sprühkompaktierter Kupferlegierungen, in: K. Bauckhage, V. Uhlenwinkel (Eds.), in: Kolloquium des SFB 372, Vol. 1, Universität Bremen, 1996, pp. 33–56, ISBN 3-88722-363-2.

[3] C. Spiegelhauer, A.S. Dan Spray, State of art for making tool steel billets by spray forming, in: K. Bauckhage, V. Uhlenwinkel (Eds.), in: Kolloquium des SFB 372, Vol. 5, Universität Bremen, 2001, pp. 63–68, ISBN 3-88722-508-2.

[4] E.J. Lavernia, Y. Wu, Spray Atomization and Deposition, Wiley, Chichester, 1996.

[5] X. Liang, J.C. Earthman, E.J. Lavernia, On the mechanism of grain formation during spray atomization and deposition, Acta Metall. Mater. 40 (11) (1992) 3003–3016.

[6] W.D. Cai, E.J. Lavernia, Modeling of porosity during spray forming, Materials Sci. Engrg. A (1997) 226–228, 8–12.

[7] P. Mathur, D. Apelian, A. Lawley, Analysis of the spray deposition process, Acta Metall. 37 (2) (1989) 429–443.

[8] D. Bergmann, U. Fritsching, K. Bauckhage, A mathematical model for cooling and rapid solidification of molten metal droplets, Internat. J. Therm. Sci. 39 (2000) 53–62.

[9] D. Bergmann, U. Fritsching, K. Bauckhage, Averaging thermal conditions in molten metal sprays, in: B. Mishra (ed.), Proc. TMS—Annual Meeting, EPD Congress, San Diego USA, February 28 – March 4, 1999, pp. 129–138.

[10] P.S. Grant, B. Cantor, L. Katgerman, Modelling of droplet dynamic and thermal history during spray forming—I. Individual droplet behaviour, Acta Mater. 41 (11) (1993) 3097–3108.

[11] M. Buchholz, V. Uhlenwinkel, N. Ellendt, The effect of deposition temperature on the sticking efficiency during spray forming, in: Proc. International Conference on Spray Forming, Baltimore USA, September 1999, pp. 13–15.

[12] K.P. Mingard, P.W. Alexander, S.J. Langride, G.A. Tomlinson, B. Cantor, Direct measurement of sprayform temperatures and the effect of liquid fraction on microstructure, Acta Mater. 46 (10) (1998) 3511–3521.

[13] S. Annavarapu, D. Apelian, A. Lawley, Spray casting of steel strip: Process analysis, Metallurgical Trans. A 21 (1990) 3237–3256.

[14] D.H. Chang, S. Kang, Analysis of transient heat conduction with phase change in a spray deposited body, in: S.P. Marsh, J.A. Dantzig et al. (Eds.), Solidification, TMS Annual Meeting in San Antonio, Warrendale, Texas, February 15–19, 1998, pp. 497–507.

[15] P. Mathur, S. Annavarapu, D. Apelian, A. Lawley, Spray casting: An integral model for process understanding and control, Material Sci. Engrg. A 142 (1991) 261–276.

[16] J.E. Fischer, V. Uhlenwinkel, R. Schröder, N. Jordan, S. Hansmann, H.R. Müller, Thermal cracking in large diameter spray formed billets, Internat. J. Powder Metallurgy 35 (6) (1999) 27–34.

[17] H. Zhang, Temperaturverteilung im aufwachsenden Deposit und im Substrat sowie Verläufe des Erstarrungsgrades im Deposit bei der Sprühkompaktierung von Metallen, Dissertation, Universität Bremen, 1994.

[18] R. Schröder, R. Kienzler, Numerische Untersuchungen an sprühkompaktierten bolzenförmigen Deposits, in: K. Bauckhage, V. Uhlenwinkel (Eds.), in: Kolloquium des SFB 372, Vol. 3, Universität Bremen, 1998, pp. 93–114, ISBN 3-88722-419-1.

[19] S. Ho, E.J. Lavernia, Thermal residual stresses in spray atomized and deposited Ni_3Al, Scripta Mater. 34 (4) (1996) 527–536.

[20] V.R. Voller, C.R. Swaminathan, B.G. Thomas, Fixed grid techniques for phase change problems: A review, Internat. J. Numer. Methods Engrg. 30 (1990) 875–898.

[21] V.R. Voller, C.R. Swaminathan, General source-based method for solidification phase change, Numer. Heat Transfer B 19 (1991) 175–189.
[22] C. Prakash, V. Voller, On the numerical solution of continuum mixture model equations describing binary solid-liquid phase change, Numer. Heat Transfer B 15 (1989) 171–189.
[23] H.D. Baehr, K. Stephan, Wärme- und Stoffübertragung, 2. Auflage, Springer-Verlag, Berlin, 1996.
[24] D. Bergmann, Modellierung des Sprühkompaktierprozesses für Kupfer- und Stahlwerkstoffe, Dissertation, Universität Bremen, 2001.
[25] J.F. Thomson, Z.U.A. Wari, C.M. Mastin, Numerical Grid Generation, Elsevier, Amsterdam, 1985.
[26] K.P. Mingard, B. Cantor, I.G. Palmer, I.R. Hughes, P.W. Alexander, T.C. Willis, J. White, Macro-segregation in aluminium alloy spray-formed billets, Acta Mater. 48 (2000) 2435–2449.
[27] M. Buchholz, V. Uhlenwinkel, A. Freyberg, K. Bauckhage, Specific enthalpy measurement in molten metal spray, in: Conference on Spray Deposition and Melt Atomization, Vol. 2, June 26–28, Bremen, Germany, 2000, pp. 703–714.
[28] D. Kurt, Kupfer und Kupferlegierungen in der Technik, Springer-Verlag, Berlin, 1967.
[29] Y.S. Touloukian, et al., Thermal Radiative Properties, Metallic Elements and Alloys, in: Thermal Physical Properties of Matter, Vol. 7, IFI/Plenum, New York, 1970.
[30] F. Richter, Die physikalischen Eigenschaften von metallischen Werkstoffen, Metall 6 (1991) 582–589.
[31] Material properties database of the spray forming research centre, SFB 372, University of Bremen, Germany.
[32] Y.S. Touloukian, et al., Thermal Conductivity, Metallic Elements and Alloys, in: Thermal Physical Properties of Matter, Vol. 1, IFI/Plenum, New York, 1970, ISBN: 0-306-67021-6.
[33] Verein Deutscher Ingenieure VDI, VDI-Wärmeatlas, 8. Auflage, Springer-Verlag, Berlin, 1997.
[34] D.A. Porter, K.E. Easterling, Phase Transformations in Metals and Alloys, 2nd Edition, Chapman & Hall, London, 1992.
[35] C. Kramer, Die Kompaktierungsrate beim Sprühkompaktieren von Gaußförmigen Deposits, Dissertation, Universität Bremen, 1997.